Supplementary Figures

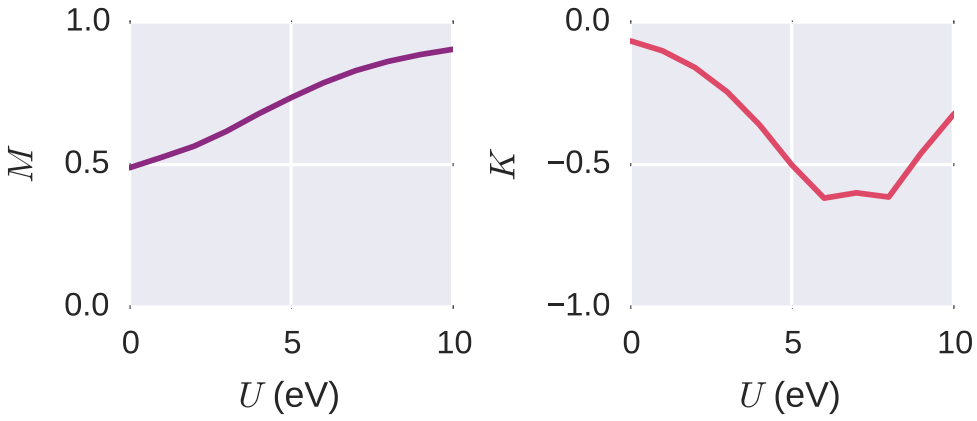

Supplementary Figure 1: The effective magnetic moment $M = \sqrt{\langle \mathbf{S}_1^2 \rangle / 3}$ (normalised by saturation value) and the spin correlation $K = 2\langle \mathbf{S}_1 \cdot \mathbf{S}_2 \rangle$ for varying values of the Hubbard U. For a pure two orbital singlet, $K = -1.5$. In our calculations, as the rest of the molecule hybridises with the Cu orbitals, the spin-correlation is re-normalised to half its saturation value for $U = 6 - 8\,\text{eV}$.

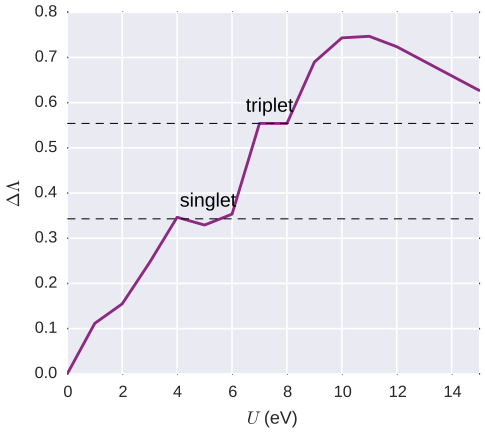

Supplementary Figure 2: The Von Neumann entropy Λ of the reduced density matrix and its dependence on the on-site interaction U.

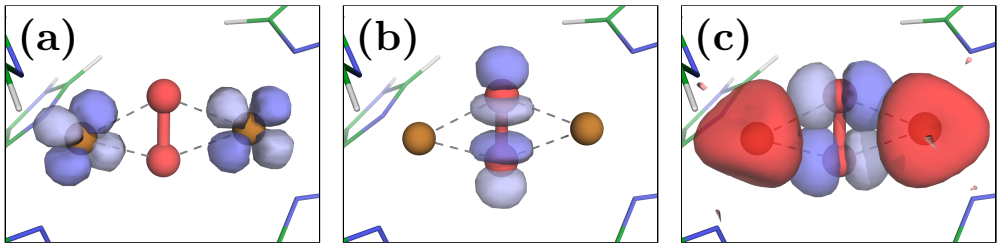

Supplementary Figure 3: Isosurfaces of several natural bonding orbitals for $U = 8\,\text{eV}$. (a) Two Cu $3d$ orbitals are identified as half-filled by the NBO analysis. (b) The O_2 σ^* anti-bond is empty, and does not hybridise with any Cu orbitals. (c) Instead, O $2p$ (blue) to Cu $4s$ (red) charge transfer is favourable.

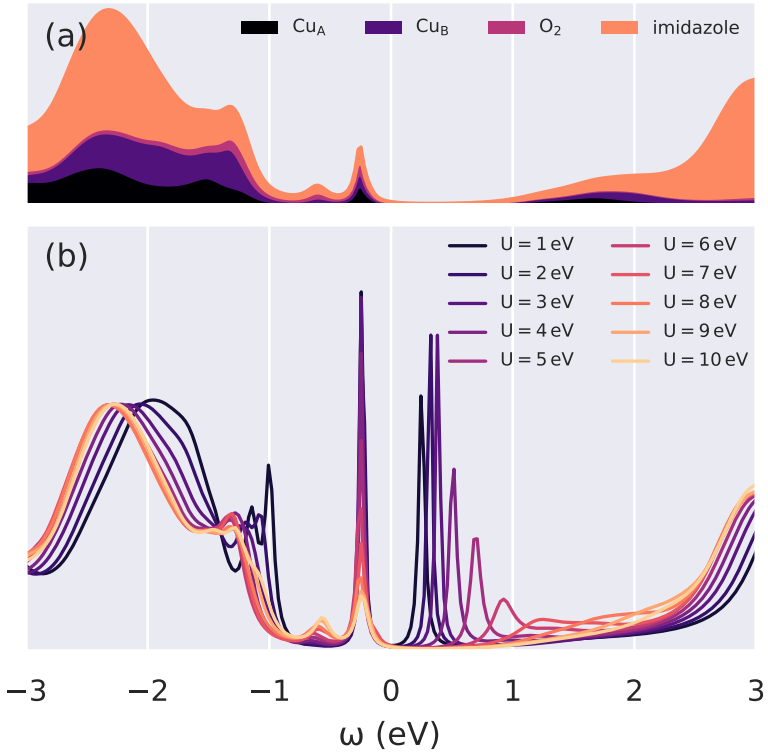

Supplementary Figure 4: (a) The local density of states for $U = 8\,\text{eV}$ and (b) the different total density of states of the Cu_2O_2 functional complex for a range of Hubbard U values from DMFT.

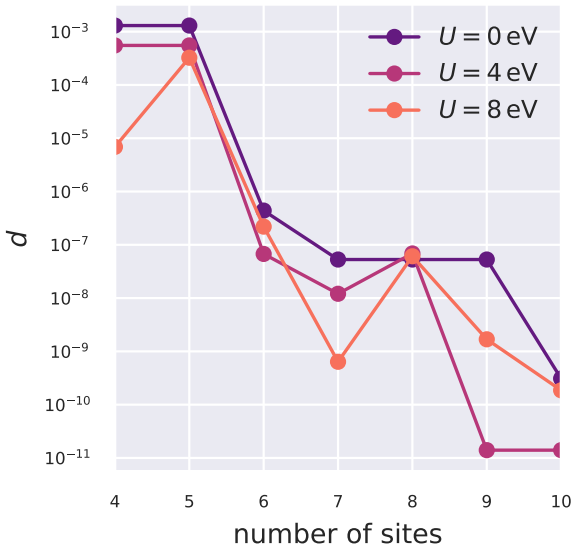

Supplementary Figure 5: The convergence of the distance d as a function of the total number of sites (impurity and bath).

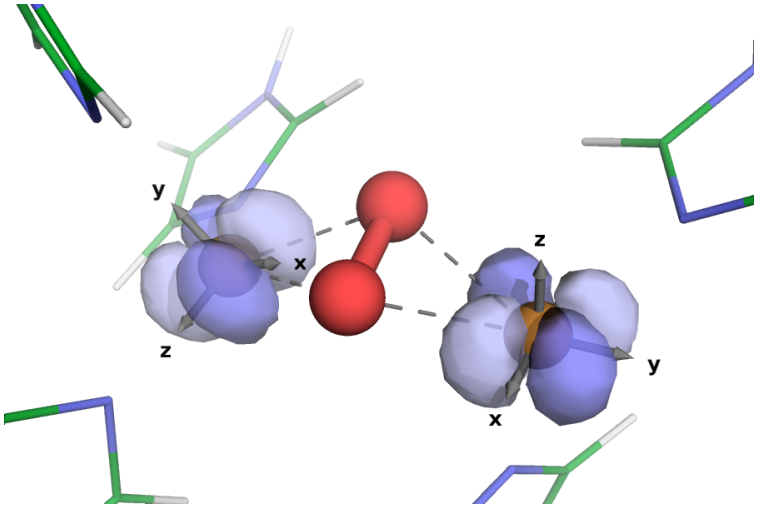

Supplementary Figure 6: The local axes for the Cu $3d$ correlated subspaces, and the two half-filled NBOs for comparison.

Supplementary Table

Supplementary Table 1: The DMFT $3d$ orbital occupations of Cu in our model of ligated hemocyanin for different Hubbard U values, as calculated using NBO. Note that the orbital labels correspond to the local axes to each Cu atom (Supplementary Figure 6). All eight other Cu $3d$ orbitals had occupancies > 1.98 for all values of U.

	U (eV)			
	0	4	6	8
Cu_A d_{xz}	1.55	1.47	1.27	1.17
Cu_B d_{xy}	1.59	1.51	1.22	1.13

Supplementary Note 1: Details of diamagnetism

The effective magnetic moment and spin correlation of the Cu dimer are shown in Supplementary Figure 1. The spin correlation K reaches half the saturation value for $U = 6 - 8\,\text{eV}$. Note that the saturation value would only be obtained for a diatomic system in vacuum, which is not hybridised to the rest of the molecule. As the local Cu $3d$ orbital charge and spin are not true quantum numbers in the molecule due to hybridisation, quantum fluctuations reduce the amplitude of the spin correlation to half the full value. This is consistent with the presence of approximately 50% combined d^{19} and d^{20} excitations (Figure 3 of the main text).

Supplementary Note 2: Von Neumann entropy

The importance of multi-determinental physics can be quantified by the Von Neumann entropy. This provides a measure to identify the degree to which the system is in a mixed quantum state with a multitude of significant components. The Von Neumann entropy, obtained in the di-Cu $3d$ subspace, is given by $\Lambda = \text{Tr}\,[\hat{\rho}_d \log \hat{\rho}_d]$, where $\hat{\rho}_d$ is the di-Cu reduced finite-temperature density matrix, traced over the states of the AIM bath environment (Supplementary Figure 2). Interestingly,

we find that the entanglement entropy increases monotonically in the range $U = 0 - 10\,\text{eV}$. We note the presence of two plateaus, for $U = 4 - 6\,\text{eV}$ and $U = 7 - 8\,\text{eV}$, that coincide with the formation of the singlet and triplet configurations in the histogram in Figure 3 of the main text.

Supplementary Note 3: Natural bond orbital analysis

In order to understand the nature of the bonding in the Cu_2O_2 complex, natural bond orbital (NBO) analysis was performed on the DFT and DMFT electronic densities.[1] This involves a series of diagonalisation and occupancy-weighted orthogonalisation procedures on the single-particle density matrix, transforming it into a set of atom-centered orthogonal natural atomic orbitals (NAOs), then natural hybrid orbitals, and finally the natural bond orbitals $\{|\sigma_i\rangle\}$, which are either one- or two-atom centered. By construction, this procedure decomposes the electronic density into terms resembling Lewis-type chemistry (with bonding and lone pairs of electrons). The NBOs generated from DFT + DMFT densities largely retain the familiar profile of DFT-based NBOs, but their occupancies may be expected to deviate further from integer values due to quantum-mechanical and finite-temperature multi-reference effects captured within DFT + DMFT.

Natural bond orbital analysis was performed using the *NBO 5* programme.[2] Performing this transformation starting from ONETEP's basis of NGWFs is described by Lee *et al.*[3] This analysis reveals a hole in one $3d$ orbital for each Cu atom (with $3d$ occupancies of 9.11 and 9.07 for $U = 8\,\text{eV}$), confirming the expected Cu(II) oxidation state $3d^9 4s^0$ (Supplementary Table 1 and Supplementary Figure 3a).

A second-order perturbation analysis detects multiple energetically favourable transfers of electronic density from filled to unfilled NBOs, revealing those aspects of the electronic structure that are not well described by Lewis-like chemistry. Early studies of hemocyanin identified back-bonding charge transfer from Cu $3d$ to oxygen σ^* anti-bonding orbitals (Supplementary Figure 3b) as an important factor in explaining the comparatively low $750\,\text{cm}^{-1}$ Raman frequency of the O_2 bond.[4] However, our second-order perturbation analyses find that this back-transfer is not present.

For $U = 8\,\text{eV}$ we instead detect favourable charge transfer from O $2p$ orbitals to Cu $4s$ orbitals (Supplementary Figure 3c).

Supplementary Note 4: Atomic coordinates of the model system

The atomic coordinates (in Angstroms) of the model system are listed below and published separately in an xyz file. This is the QM region of the QM/MM region of Supplementary Ref. 5 optimised using the B3LYP hybrid functional. It closely matches the geometry of the Cu_2O_2 core in XRD measurements of oxyHc and oxyTy.

N	16.51891392	15.23078843	9.22976689
H	16.93119882	15.08539696	8.30438809
C	16.94902112	16.13114758	10.17383386
N	15.18637912	14.99749680	10.95580106
C	16.10933852	15.98208447	11.24036986
H	16.10095092	16.50742455	12.17967036
C	15.45961072	14.56963464	9.73009877
H	14.93592812	13.80224391	9.18792729
N	15.68221352	11.68923875	15.07079896
H	15.62223022	10.91935273	15.75177196
C	16.82912232	12.31709786	14.63750076
N	15.03728172	13.21411391	13.63477906
C	16.41234182	13.26768084	13.74798876
H	16.99541732	13.97028085	13.18028166
C	14.63155912	12.24369975	14.44250686
H	13.62176392	11.89057990	14.57154846
N	11.20316861	16.38796731	14.67452056
H	10.83895228	16.68400689	15.58698756
C	10.65158961	16.72090836	13.45946316
N	12.41187546	15.35470124	13.15331656
C	11.41667864	16.07778569	12.52477076
H	11.32106945	16.09724541	11.45289136
C	12.25019047	15.56909772	14.44942096
H	12.86310074	15.16461678	15.23767766

N	9.49463341	9.86374493	13.93094066
H	9.73159525	9.00103207	14.43246936
C	8.24884198	10.31835957	13.54789546
N	9.84466860	11.48322602	12.50309476
C	8.48328564	11.32677766	12.65632446
H	7.78488610	11.93928595	12.11399846
C	10.42165444	10.58129044	13.27870086
H	11.47834322	10.42322846	13.40566166
N	12.01234028	9.47930928	8.02845959
H	12.68808052	9.09180375	7.36268858
C	11.00609562	8.75784417	8.62913327
N	11.09392331	10.81562920	9.51444153
C	10.43873522	9.60240193	9.54022602
H	9.61370823	9.41996499	10.20636756
C	12.04142449	10.69948407	8.60142712
H	12.77187130	11.45055695	8.35522084
N	8.61465523	14.51152774	8.41694931
H	8.38643811	14.76536198	7.45209746
C	8.18880818	15.20575448	9.51961235
N	9.53424857	13.53805896	10.13587576
C	8.76071236	14.58675404	10.59130386
H	8.67891762	14.82165976	11.63805866
C	9.42431137	13.52365895	8.81797604
H	9.92450163	12.84226676	8.15381340
Cu	10.90108130	12.43349095	11.08418656
Cu	13.85734532	14.03834172	12.18094446
O	12.72653935	12.32631179	11.81473546
O	12.74707482	13.23837395	10.72427086
H	17.81251122	16.77851220	10.02095606
H	17.81738922	12.01153775	14.98105336
H	9.84447262	17.44637512	13.35784536
H	7.32911179	9.83963986	13.88403226
H	10.86685059	7.70012590	8.40572647
H	7.51362297	16.05692406	9.43184952

Supplementary Note 5: Convergence of the system-to-AIM mapping

In DMFT, the accurate mapping of the physical system to an Anderson Impurity Model (AIM) is crucial. This mapping is achieved by fitting the AIM hybridisation function $\Delta_{\text{imp}}(\omega)$ to the hybridisation function of the physical system $\tilde{\Delta}(\omega)$, where these hybridisation functions are defined as $\Delta(\omega) = \omega + \mu - t - G^{-1}(\omega) - \Sigma(\omega)$ (where μ is the chemical potential, t the d-d hopping parameters, G the one-particle Green's function and Σ the self-energy). In the impurity Green's function of an AIM, all of the parameters associated with the bath orbitals only appear via the hybridisation function; that is, it contains all of the physics of the bath orbitals pertinent to the impurity orbitals. The matching of the hybridisation functions is achieved by minimising the function

$$d = \sum_{\omega<\omega_c} \frac{1}{\omega^\gamma} \left| \Delta_{\text{imp}}(\omega) - \tilde{\Delta}(\omega) \right|^2 \tag{1}$$

with respect to the AIM parameters. ω_c is a cutoff frequency and γ is a user-specified parameter that can allow for preferential weighting of agreement at low frequencies. If we increase the number of sites of our AIM, the AIM Hamiltonian has more parameters, and we stand a better chance of fitting the physical hybridisation function because the AIM hybridisation function is more flexible. Supplementary Figure 5 shows the convergence of the distance d as a function of the total number of sites in the AIM. We note that as a rule of thumb $d < 10^{-7}$ is generally adequate; if d is much smaller than this it tends to indicate overfitting. The calculations in this work used eight sites.

Supplementary Note 6: Local axes

The local axes for the two Cu subspaces are shown in Supplementary Figure 6. This particular rotation minimises the off-diagonal elements of the local Green's function. As shown in Supplementary Table 1 these axes localise the holes on single d orbitals; d_{xz} for Cu_A (on the left of the figure) and d_{xy} for Cu_B (on the right). The two NBOs identified as being half-filled are plotted for comparison. Since the NBO analysis is agnostic to the projection procedure used in the cluster DMFT calculations, it is reassuring that these orbitals align with the axes.

Supplementary References

1. Reed, A. E., Curtiss, L. A. & Weinhold, F. Intermolecular interactions from a natural bond orbital, donor-acceptor viewpoint. *Chem. Rev.* **88**, 899–926 (1988).

2. Glendening, E. D. *et al.* NBO 5.9 and the NBO 5.9 Manual (2011). URL `https://nbo6.chem.wisc.edu/`.

3. Lee, L. P., Cole, D. J., Payne, M. C. & Skylaris, C.-K. Natural bond orbital analysis in the ONETEP code: applications to large protein systems. *J. Comp. Chem.* **34**, 429–444 (2013).

4. Baldwin, M. J. *et al.* Spectroscopic studies of side-on peroxide-bridged binuclear copper(II) model complexes of relevance to oxyhemocyanin and oxytyrosinase. *J. Am. Chem. Soc.* **114**, 10421–10431 (1992).

5. Saito, T. & Thiel, W. Quantum mechanics/molecular mechanics study of oxygen binding in hemocyanin. *J. Phys. Chem. B* **118**, 5034–5043 (2014).